



# Percussion characteristic analysis for hydraulic rock drill with no constant-pressurized chamber through numerical simulation and experiment

Wei Ma<sup>1</sup> , Xiaoguang Geng<sup>2</sup> , Chengzhe Jia<sup>3</sup>, Lulu Gao<sup>2</sup>,  
Yuchao Liu<sup>2</sup> and Xiang Tian<sup>2</sup>

## Abstract

Considering the insufficiency of numerical study on the percussion characteristic of hydraulic rock drill, which restricts the improvement of efficiency and reliability, a coupling model including the impact piston, spool valve, impact accumulator, and connecting pipelines was established taking into account the oil compressibility, oil leakage, and pressure drop in valve ports. The rebound velocity of impact piston was calculated based on the stress wave theory. The simulation results revealed the coupling mechanism of percussion system. Pressure curves of the piston's front-chamber and rear-chamber, and valve's left-chamber and right-chamber were obtained by field rock drilling test. Then, the velocity curve of impact piston was obtained after judging the striking point through the feature of rear-chamber's pressure spike, so were the rock drill's impact energy, impact frequency, and impact power. The simulation and experimental results have consistency. And, on this basis, the influence of spool valve's damping clearance ( $\delta$ ) and pipeline diameters ( $d_1, d_2$ ) connecting the impact piston and spool valve on the percussion performance and system cavitation was researched. The results show that the larger  $\delta$  is better considering reversal time of spool valve, the impact frequency of rock drill, pressure fluctuation, and cavitation relief. But too large  $\delta$  will cause over quick impact velocity of the spool valve, which may lead to strong vibration and the damage of spool valve. The optimal value of  $\delta$  is 0.01 mm by comprehensive consideration. The pipeline diameters have an important influence on the pressure fluctuation and negative pressure in rear-chamber. The diameters should be larger than 18 mm to alleviate the cavitation. This article provides means for the design and research of rock drills.

## Keywords

Hydraulic rock drill, no constant-pressurized chamber, percussion characteristic, numerical simulation, field rock drilling test

Date received: 9 October 2018; accepted: 8 March 2019

Handling Editor: Wenwu Xu

## Introduction

In recent years, hydraulic rock drills have been widely used in many applications, such as mining, coal mine roadway excavation, railway tunnel, highway tunnel, and rock excavation projects because of their high efficiency, clean, and safety.<sup>1,2</sup> The hydraulic rock drill

<sup>1</sup>School of Civil and Resource Engineering, University of Science and Technology Beijing, Beijing, China

<sup>2</sup>School of Mechanical Engineering, University of Science and Technology Beijing, Beijing, China

<sup>3</sup>College of Mechanical Engineering and Applied Electronics Technology, Beijing University of Technology, Beijing, China

### Corresponding author:

Xiaoguang Geng, School of Mechanical Engineering, University of Science and Technology Beijing, Beijing 100083, China.

Email: ustbgxg@163.com



with high frequency and high power becomes the first choice facing the scale of mining and larger-scale tunneling.<sup>3,4</sup> Different from the DTH (down-the-hole) hammers,<sup>5–7</sup> the hydraulic rock drill is driven by hydraulic system and belongs to top hammer drilling. As the core component of rock drill, the performance of percussion system decides the whole level of rock drill to a great extent.<sup>8,9</sup> However, the structure of percussion system is complicated, and its working process obeys the hydraulic–mechanical–pneumatic coupling laws,<sup>10</sup> which introduces great difficulty in researching on the percussion characteristic of hydraulic rock drill.

J Seo and colleagues<sup>11–13</sup> developed an analysis model for rock drill using SimulationX software, which was validated by the static calibration and measurement tests of impact frequency and impact energy under three different supply pressure conditions. Based on a simulation model for rock drill built by AMESim, JY Oh et al.<sup>14</sup> studied the dynamic performance of percussion system and effects of rock hardness on it. JY Oh et al.<sup>15</sup> also investigated the influence of percussion system parameters on percussion performance and found that the impact power was affected by supply pressure, areas of the impact piston and shuttle valve, and position of the hydraulic port strongly. Q Hu et al.<sup>16</sup> studied the percussion performance of rock drill with single-degree-of-freedom impact oscillator model and revealed that the simulation results were consistent with stress wave test results. S Yang and colleagues<sup>17–19</sup> analyzed the percussion performance of rock drill and optimized the parameters with simulation model, which was validated by the percussion performance test. C Song et al.<sup>20</sup> optimized the design parameters of percussion system for rock drill using Taguchi method. Y Li et al.,<sup>21</sup> J Hu and Q Hu,<sup>22</sup> and H Zhao et al.<sup>23</sup> analyzed the influence of the opening at zero position of distribute valve on the internal motion law for the hydraulic rock drill. W Ding and X Huang<sup>24</sup> established a hydraulic impactor simulation system based on the theory of bond graph in AMESim software. Z Zhou et al.<sup>25</sup> and Z Yin and Y Hu<sup>26</sup> studied the dynamic characteristics of a percussion system using AMESim and obtained motion law of the impact piston and spool valve. Z Wen et al.<sup>27</sup> built a simulation model for a percussion system and studied the effects of some factors on the percussion performance.

The previous research works on percussion system are mostly the simulation analysis, and the simulation models are too simplified. The simulation results are quite different from the actual condition. There are many problems including cavitation erosion of impact piston and bush, impact powerless of the rock drill, and so on, which cannot be researched by simulation. For this reason, a coupling model including impact piston,

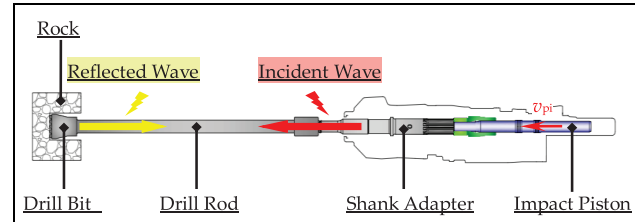


**Figure 1.** Schematic diagram of the percussive drilling.

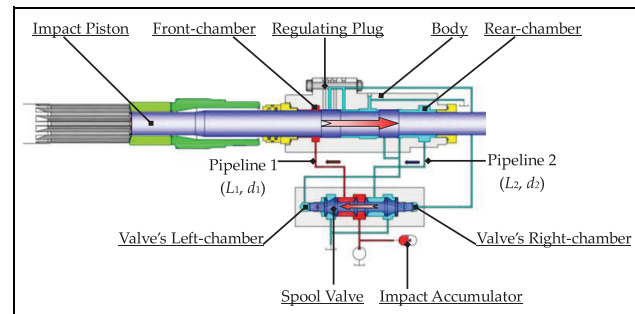


**Figure 2.** Schematic diagram of the percussion system.

spool valve, impact accumulator, and connecting pipelines will be established considering the oil compressibility, oil leakage, and pressure drop in valve ports. The rebound velocity of impact piston will be calculated based on the stress wave theory. The field rock drilling test will be conducted to verify the numerical model by contrasting the change law of pressure and percussion performance by simulation and experiment. Above all, the influencing factors on the percussion characteristic of rock drill will be researched.

## Working principle of hydraulic rock drill

Figure 1 shows the schematic diagram of percussive drilling. Under the action of percussion system, the impact piston hits the shank adapter with high frequency and high speed. Its kinetic energy is transmitted to rock through shank adapter, drill rod, and drill bit in the form of stress wave. The impact piston will rebound under the reflected wave because of the difference in wave resistance.

As shown in Figure 2, the percussion system with no constant-pressure chamber is mainly composed of an impact piston, a spool valve, an impact accumulator, a regulating plug, and a body. The impact piston connects the spool valve with pipeline 1 and pipeline 2. Their movement obeys the principle of hydraulic slave. The pressure in front-chamber and rear-chamber exchanges under a certain frequency. The frequency of rock drill can be adjusted through the regulating plug.

## Coupling model of percussion system

### Stress wave model

The solving equation of incident wave is as follows<sup>28</sup>

$$P_r = \begin{cases} \frac{Z_h \cdot Z_q}{Z_h + Z_q} v_{pp}, & 0 < t < t_h \\ \frac{Z_h \cdot Z_q}{Z_h + Z_q} \left( \frac{Z_h - Z_q}{Z_h + Z_q} \right) v_{pp}, & t > t_h \end{cases} \quad (1)$$

where  $P_r$  is the incident stress wave (Pa);  $Z_h$  and  $Z_q$  are the wave resistance ( $\text{Ns m}^{-1}$ ) of impact piston and shank adapter, respectively;  $v_{pp}$  is the last impact velocity of impact piston ( $\text{m s}^{-1}$ ); and  $t_h$  is the duration of incident wave (s).

The wave resistance of the impact piston and shank adapter are equal, namely,  $Z_h = Z_q = Z$ . So

$$P_r = \begin{cases} \frac{1}{2} Z v_{pp}, & 0 < t < t_h \\ 0, & t > t_h \end{cases} \quad (2)$$

Among them

$$\begin{cases} t_h = 2 \cdot \frac{L_h}{c} \\ Z = A \cdot \sqrt{E\rho} \\ c = \sqrt{\frac{E}{\rho}} \end{cases} \quad (3)$$

where  $L_h$  is the length of impact piston (m);  $c$  is the wave velocity ( $\text{m s}^{-1}$ );  $A$ ,  $E$ , and  $\rho$  are the cross sectional area ( $\text{m}^2$ ), elastic modulus (Pa), and density ( $\text{kg m}^{-3}$ ) of impact piston, respectively.

Extensive experiments<sup>4,29,30</sup> illustrate that near-linear relationship exists between the penetration force and penetration depth. So, equation (4) is satisfied

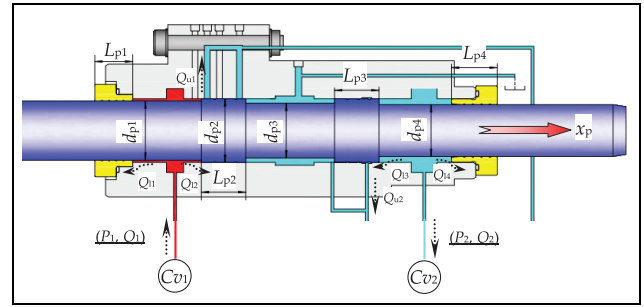


**Figure 3.** Structure diagram of the impact piston part.

Equations (6) and (7) are dynamic equations for loading and unloading section, respectively, which are obtained by uniting equations (2), (4), and (5)

$$\begin{cases} F = P_r + Q_r \\ \frac{du}{dt} = \frac{1}{Z}(P_r - Q_r) \\ F = Ku \\ t = 0, F = 0 \end{cases} \quad (6)$$

$$\begin{cases} F = P_r + Q_r \\ \frac{du}{dt} = \frac{1}{Z}(P_r - Q_r) \\ F = F_{\max} - rK(u_{\max} - u) \\ t = t_h, F = F_{\max} = Ku_{\max} \end{cases} \quad (7)$$

Then, function of reflected wave is obtained

$$Q_r = \begin{cases} \frac{1}{2} Z v_{pp} - Z v_{pp} e^{-\frac{Kt}{Z}}, & 0 < t \leq t_h \\ \left( Z v_{pp} - Z v_{pp} e^{-\frac{Kt_h}{Z}} \right) e^{-\frac{rK(t-t_h)}{Z}}, & t > t_h \end{cases} \quad (8)$$

The rebound velocity of impact piston  $\dot{x}_p(0)$  can be expressed as equation (9) according to the law of momentum conservation

$$\dot{x}_p(0) = \begin{cases} \frac{v_{pp}\lambda}{2\gamma} \cdot \left[ \left( \frac{2}{\lambda} - 1.6 \right) \cdot \gamma + 4 \cdot \gamma \cdot (e^{-\frac{2}{\lambda}} - e^{-1.6}) + 2 \cdot (1 - e^{-\frac{2}{\lambda}}) \cdot (1 - e^{-1.6\gamma}) \right], & \lambda \leq 1.25 \\ \frac{v_{pp}\lambda}{2\gamma} \cdot (e^{-\frac{2\gamma}{\lambda}} - 1) \cdot \left[ 2 \cdot (e^{-\frac{2}{\lambda}} - 1) \cdot (1 - \gamma) - \frac{2\gamma}{\lambda} \right], & \lambda > 1.25 \end{cases} \quad (9)$$

$$F = \begin{cases} Ku \\ F_{\max} - rK(u_{\max} - u) \end{cases} \quad (4)$$

where  $K$  is the load stiffness of rock ( $\text{N m}^{-1}$ );  $u$  was the penetration depth (m); and  $\gamma$  is the unload coefficient.

The wave superposition equation (5) is as follows regarding the interface surface between drill bit and rock as the research object

$$\begin{cases} F = P_r + Q_r \\ \frac{du}{dt} = \frac{1}{Z}(P_r - Q_r) \end{cases} \quad (5)$$

where  $Q_r$  is the reflected wave.

Among them

$$\lambda = \frac{Z^2}{m_p \cdot K} \quad (10)$$

### Mathematical model of impact piston

As shown in Figure 3,  $C_{v1}$  and  $C_{v2}$  are the front-chamber and rear-chamber of impact piston, respectively. Considering viscous friction and friction force of seal, the dynamic model (equation (11)) of impact piston can be established according to Newton's mechanics

$$m_p \ddot{x}_p + K_p \dot{x}_p + F_f \frac{|\dot{x}_p|}{\dot{x}_p} = A_1 P_1 - A_2 P_2 \quad (11)$$

Among them

$$\begin{cases} A_1 = \frac{\pi}{4} (d_{p2}^2 - d_{p1}^2) \\ A_2 = \frac{\pi}{4} (d_{p2}^2 - d_{p4}^2) \\ K_p = \frac{\pi\mu}{\sqrt{1-\varepsilon^2}} \left( \frac{d_{p1}L_{p1}}{h_1} + \frac{d_{p2}L_{p2}}{h_2} + \frac{d_{p2}L_{p3}}{h_3} + \frac{d_{p4}L_{p4}}{h_4} \right) \\ F_f = \pi \cdot d_{p1} \cdot b \cdot f \cdot P_1 + \pi \cdot d_{p4} \cdot b \cdot f \cdot P_2 \\ \quad + 2\pi(d_{p1} + d_{p4})\zeta \end{cases} \quad (12)$$

where  $m_p$  is the mass of impact piston (kg);  $K_p$  is the viscous friction coefficient ( $\text{kg s}^{-1}$ );  $F_f$  is the friction force of the seal (N);  $\dot{x}_p$  and  $\ddot{x}_p$  are the velocity ( $\text{m s}^{-1}$ ) and acceleration ( $\text{m s}^{-2}$ ) of impact piston, respectively.  $A_1$  and  $A_2$  are the effective area of the front-chamber and rear-chamber ( $\text{m}^2$ ), respectively.  $\mu$  is the dynamic viscosity of hydraulic oil ( $\text{kg}(\text{m s})^{-1}$ );  $\varepsilon$  is the eccentricity;  $h_i$  is the fit clearance (m) corresponding to  $L_{pi}$  ( $i = 1, 2$ , and 4);  $b$  is the seal width (mm);  $f$  is the friction coefficient between the seal and impact piston; and  $\zeta$  is the compressibility correlation coefficient of O-ring. Other parameters are shown in Figure 3.

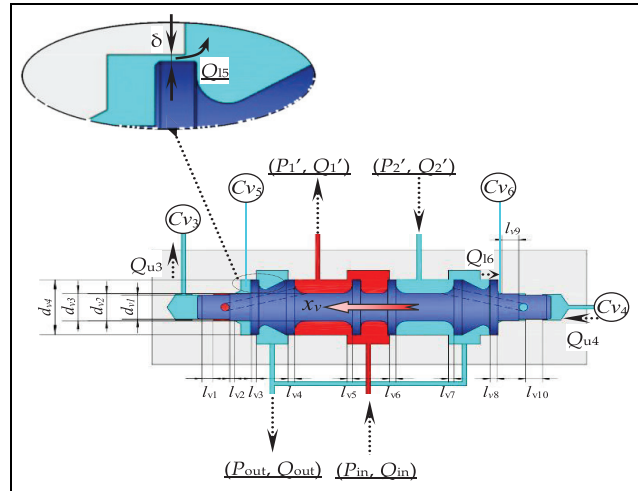
The liquid flow continuity equation of front-chamber (equation (13)) and rear-chamber (equation (14)) are established

$$\frac{V_{10} + A_1 x_p}{K_e} \cdot \frac{dP_1}{dt} = Q_{p1} - A_1 \dot{x}_p - C_3 Q_{u1} - Q_{l1} - Q_{l2} \quad (13)$$

$$\frac{V_{20} - A_2 x_p}{K_e} \cdot \frac{dP_2}{dt} = A_2 \dot{x}_p - Q_{p2} - C_4 Q_{u2} - Q_{l3} - Q_{l4} \quad (14)$$

$$\begin{cases} Q_{l1} = \frac{\pi d_{p1} h_1^3}{12 u L_{p1}} \cdot P_1 \\ Q_{l2} = \frac{\pi d_{p2} h_2^3}{12 u L_{p2}} \cdot P_1 \\ Q_{l3} = \frac{\pi d_{p2} h_3^3}{12 u L_{p3}} \cdot P_2 \\ Q_{l4} = \frac{\pi d_{p4} h_4^3}{12 u L_{p4}} \cdot P_2 \end{cases} \quad (15)$$

where  $V_{i0}$  is the initial volume ( $\text{m}^3$ ) of  $C_{vi}$  ( $i = 1, 2$ );  $K_e$  is the oil elastic modulus (MPa);  $C_3$  and  $C_4$  are variables for state judgment (0 or 1); and  $P_i$  is the pressure (Pa) corresponding to  $C_{vi}$  ( $i = 1, 2$ ). Other parameters are shown in Figure 3.



$$\frac{V_{40} + A_{v1}x_v}{K_e} \cdot \frac{dP_4}{dt} = Q_{u4} - A_{v1}\dot{x}_v \quad (19)$$

$$\frac{V_{50} - A_{v2}x_v}{K_e} \cdot \frac{dP_5}{dt} = A_{v2}\dot{x}_v - Q_{l5} \quad (20)$$

$$\frac{V_{60} + A_{v2}x_v}{K_e} \cdot \frac{dP_6}{dt} = Q_{l6} - A_{v2}\dot{x}_v \quad (21)$$

Among them

$$\begin{cases} Q_{u4} = Q_{u1}, \quad C_3 = 1 \\ Q_{u3} = -Q_{u2}, \quad C_4 = 1 \\ Q_{l5} = \frac{\pi d_{v3}\delta^3}{12ul_{v3}} \cdot (P_5 - P_{out}) \\ Q_{l6} = \frac{\pi d_{v3}\delta^3}{12ul_{v8}} \cdot (P_{out} - P_6) \\ Q_{in} = C_q \cdot A_{i1} \cdot \sqrt{\frac{P}{2} \cdot (P_{in} - P'_{i1})} \\ Q_{out} = C_q \cdot A_{i2} \cdot \sqrt{\frac{P}{2} \cdot (P'_{i2} - P_{out})} \\ A_{i1} = \pi \cdot d_{v4} \cdot l_{v5} \\ A_{i2} = \pi \cdot d_{v4} \cdot l_{v7} \end{cases} \quad (22)$$

where  $V_{i0}$  is the initial volume of  $C_{vi}$  ( $i = 3, 4, 5, 6$ ) ( $\text{m}^3$ ). Other parameters are shown in Figures 3 and 4.

### Mathematical model of impact accumulator

It is close to an isentropic process in the air chamber of impact accumulator while drilling. So, equation (23) is satisfied

$$\frac{dP_h}{dt} = \frac{1.4P_h}{V_H}Q_h \quad (23)$$

Among them

$$V_H = V_{H0} - \int_0^t Q_h dt \quad (24)$$

where  $P_h$  is the pressure in oil chamber (Pa);  $V_H$  is the gas volume ( $\text{m}^3$ );  $V_{H0}$  is the initial gas volume ( $\text{m}^3$ ); and  $Q_h$  is the flow rate into accumulator ( $\text{m}^3 \text{s}^{-1}$ ).

### Mathematical model of pipelines

The equilibrium equation and liquid flow continuity equation of pipeline 1 and pipeline 2 (Figure 2) were established considering the capacity, resistance, and inertia

$$\begin{cases} P'_1 - P_1 = R_1 \cdot Q'_1 + I_1 \cdot \frac{dQ'_1}{dt} \\ Q'_1 - Q_1 = C_1 \cdot \frac{dP'_1}{dt} \\ P_2 - P'_2 = R_2 \cdot Q_2 + I_2 \cdot \left(\frac{dQ_2}{dt}\right) \\ Q_2 - Q'_2 = C_2 \cdot \left(\frac{dP_2}{dt}\right) \end{cases} \quad (25)$$

Among them

**Table 1.** Initial parameters of the percussion system.

Parameters	Value	Parameters	Value
$m_p$	7.93 (kg)	$d_{v1}$	13 (mm)
$m_v$	0.38 (kg)	$d_{v2}$	14.5 (mm)
$d_{p1}$	46 (mm)	$d_{v4}$	30 (mm)
$d_{p2}$	50 (mm)	$h_5$	0.015 (mm)
$d_{p2}$	46 (mm)	$h_6$	0.015 (mm)
$d_{p4}$	43 (mm)	$K_e$	1700 (MPa)
$L_{p1}$	22 (mm)	$M$	$3.9 \times 10^{-2}$ ( $\text{kg}(\text{m s})^{-1}$ )
$L_{p2}$	31 (mm)	$B$	1.7 (mm)
$L_{p3}$	31 (mm)	$f$	0.05
$L_{p4}$	28 (mm)	$\zeta$	0.1
$h_1$	0.015 (mm)	$Q_{in}$	105 ( $\text{L min}^{-1}$ )
$h_2$	0.03 (mm)	$P_{in}$	20 (MPa)
$h_3$	0.03 (mm)	$\gamma$	1.5
$h_4$	0.015 (mm)	$K$	6
$\delta$	0.1 (mm)	$V_{H0}$	0.33 (L)

$$\begin{cases} R_i = \frac{128\mu L_i}{\pi d_i^4} \\ C_i = \frac{\pi d_i^2 L_i}{K} \\ I_i = \frac{\rho L_i}{\pi d_i^2} \end{cases} \quad (26)$$

where  $R_i$ ,  $C_i$ , and  $I_i$  ( $i = 1, 2$ ) are the liquid resistance, liquid capacity, and hydraulic inductance of pipelines, respectively.  $L_i$  and  $d_i$  ( $i = 1, 2$ ) are the length and diameter of pipelines, respectively.

## Numerical simulation and experimental validation

### Numerical simulation of percussion system

Table 1 shows the initial parameters of percussion system. The percussion characteristic is simulated by solving the coupling model with MATLAB software. The simulation results are shown in Figure 5.

From Figure 5, we can observe the following:

1. The high pressure alternately appears in the front-chamber and rear-chamber, namely, no constant-pressure chamber.
2. There exists pressure fluctuation in chambers because of high-frequency and high-velocity reciprocating motion of the impact piston and spool valve, and the peak pressure of rear-chamber can reach 30 MPa during the braking phase of impact piston. The pressure of rear-chamber will drop sharply when hydraulic oil comes into left-chamber of the valve and then a pressure spike appears because of impact piston's rebound.
3. The reversal time of spool valve is about 2 ms, and there exists deceleration before destination.

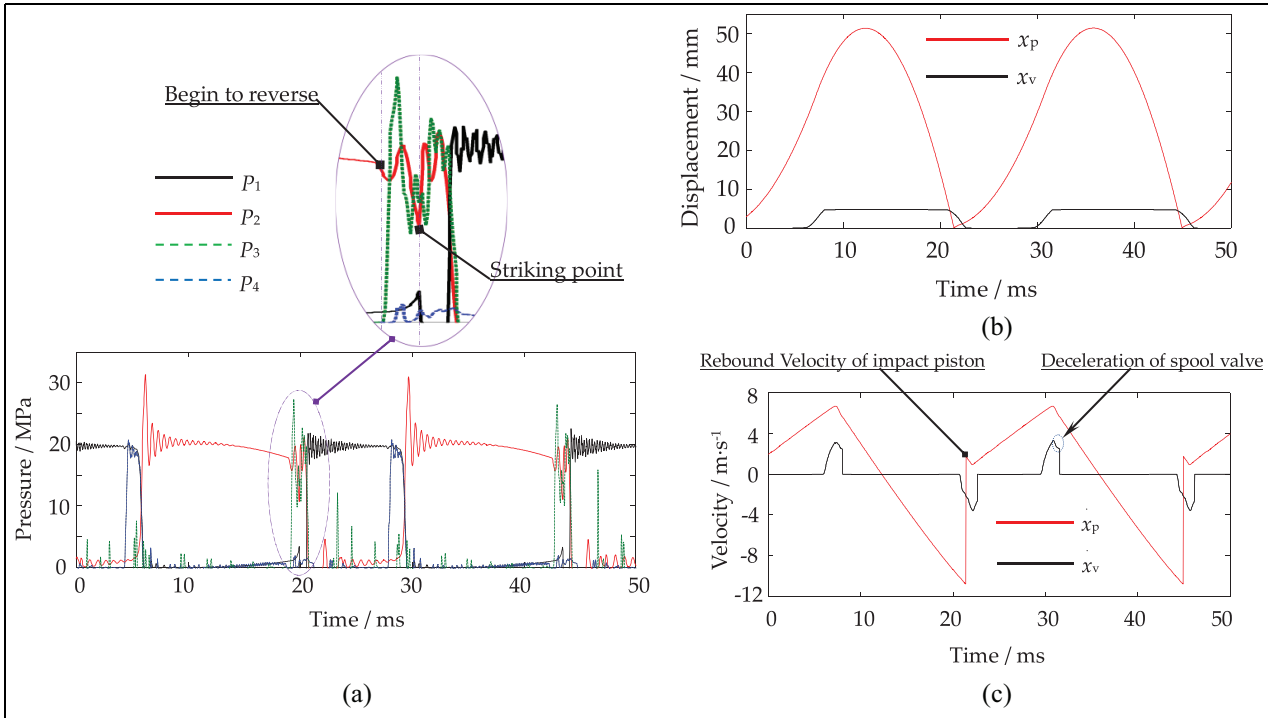


**Figure 5.** Simulation results of the percussion system: (a) pressure curves of impact piston's front-chamber and rear-chamber, valve's left-chamber and right-chamber; (b) displacement curves of the impact piston and spool valve; and (c) velocity curves of the impact piston and spool valve.

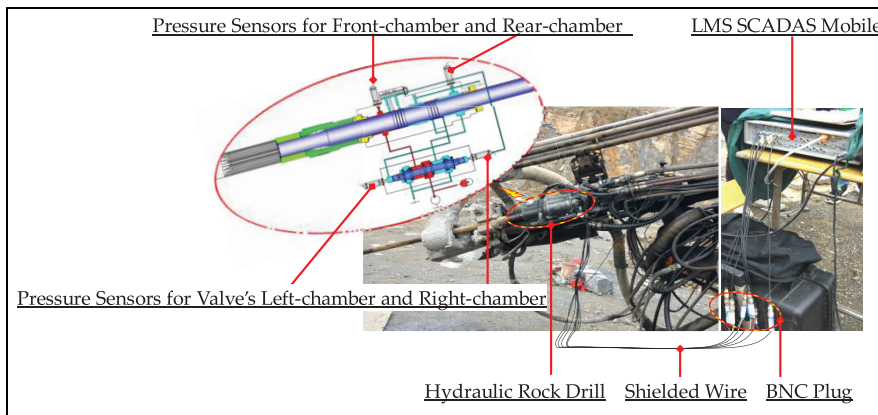


**Figure 6.** Scene graph of the field rock drilling test.

### Field rock drilling test

As shown in Figure 6, the rock drill was mounted in a drill rig. Pressure sensors were installed on the housing. The pressure in the impact piston's front-chamber and rear-chamber, and valve's left-chamber and right-chamber was tested synchronously. The sampling frequency could reach 204.8 kHz with 40 opening channels using the LMS SCADAS Mobile. The software for signal acquisition was the LMS Test Xpress 7A. Pressure sensors were the Titanium Electronic Equipment

Company's PPM-S114A type, whose response frequency was 100 kHz. Pressure signals were transmitted to the test system via shielded wire and BNC plug.

### Simulation model validation using experimental results

**Pressure curves.** The comparison of pressure curves by experiment and simulation is shown in Figure 7. We can observe that they have consistency in frequency,

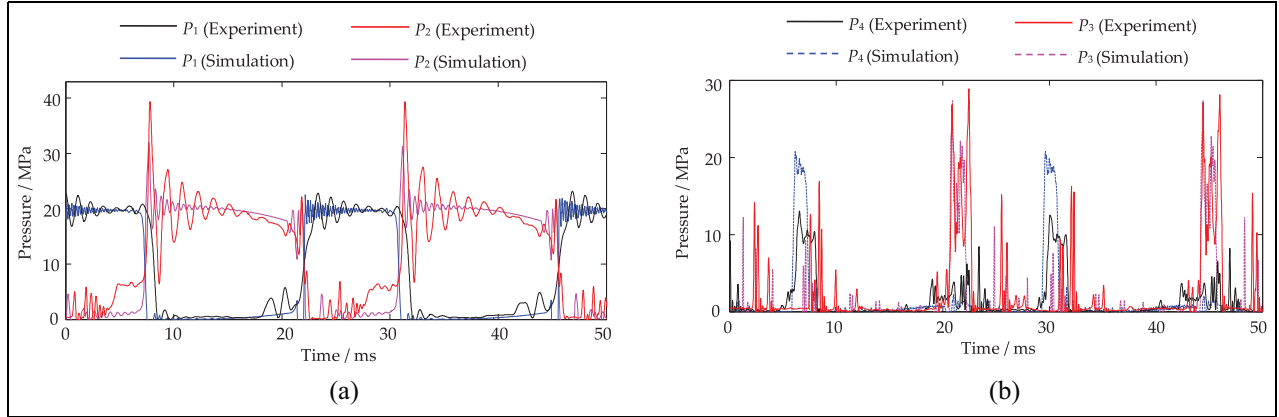


**Figure 7.** Correlation curves by experiment and simulation: (a) pressure curves of impact piston's front-chamber and rear-chamber; (b) pressure curves of valve's left-chamber and right-chamber.

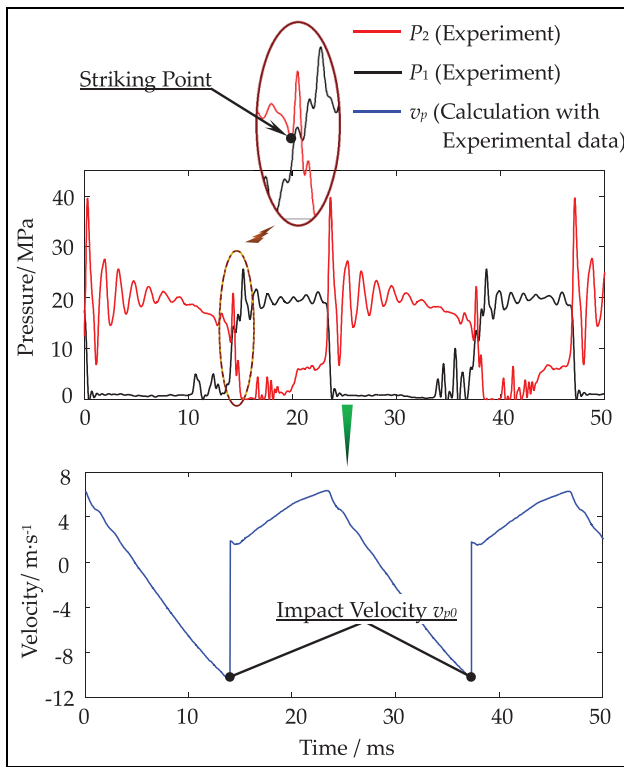


**Figure 8.** Testing curve of the pressure in chambers and velocity curve of the impact piston calculated with experimental data.

amplitude, and change law. The wave frequencies of \$P\_1\$ and \$P\_2\$ were different due to the spatial structure of the chambers, so was the return oil pressure of \$P\_2\$.

**Percussive performance.** The kinetic equation (27) of impact piston is established. The striking point can be judged through the feature of rear-chamber's pressure spike because of impact piston's rebound. Then, the

**Table 2.** Error rate between simulation and experimental results of the percussion performance.

	Impact velocity	Impact energy	Impact frequency
Measurement	\$10.47 \text{ m s}^{-1}\$	\$434.76 \text{ J}\$	\$42.35 \text{ Hz}\$
Simulation	\$10.77 \text{ m s}^{-1}\$	\$460.03 \text{ J}\$	\$42.55 \text{ Hz}\$
Error rate	2.87%	5.81%	0.47%

velocity curve of impact piston can be obtained by feeding pressure data of front-chamber and rear-chamber into equations (11), (12), and (27), which is shown in Figure 8. After that, the impact velocity can be obtained and so are the impact energy, impact frequency, and impact power

$$\begin{cases} \dot{x}_p = \dot{x}_{p0} + \int_0^t \ddot{x}_p dt \\ x_p = x_{p0} + \int_0^t \dot{x}_p dt \\ \int_0^T \dot{x}_p dt = 0 \end{cases} \quad (27)$$

Table 2 contains relative deviations between experimental and simulation results. The impact velocity of piston by simulation was higher due to the difference of return oil pressure by experiment and simulation. But the error rates are all less than 10% and even the error rate of impact frequency is 0.47%, which verifies the rationality and correctness of the simulation model.

### Analysis on factors influencing percussion characteristic

Y Li et al.<sup>31</sup> found that the damping clearance of the spool valve ( $\delta$ ) is closely related to the percussion



**Figure 9.** Cavitation erosion of the impact piston and bush.

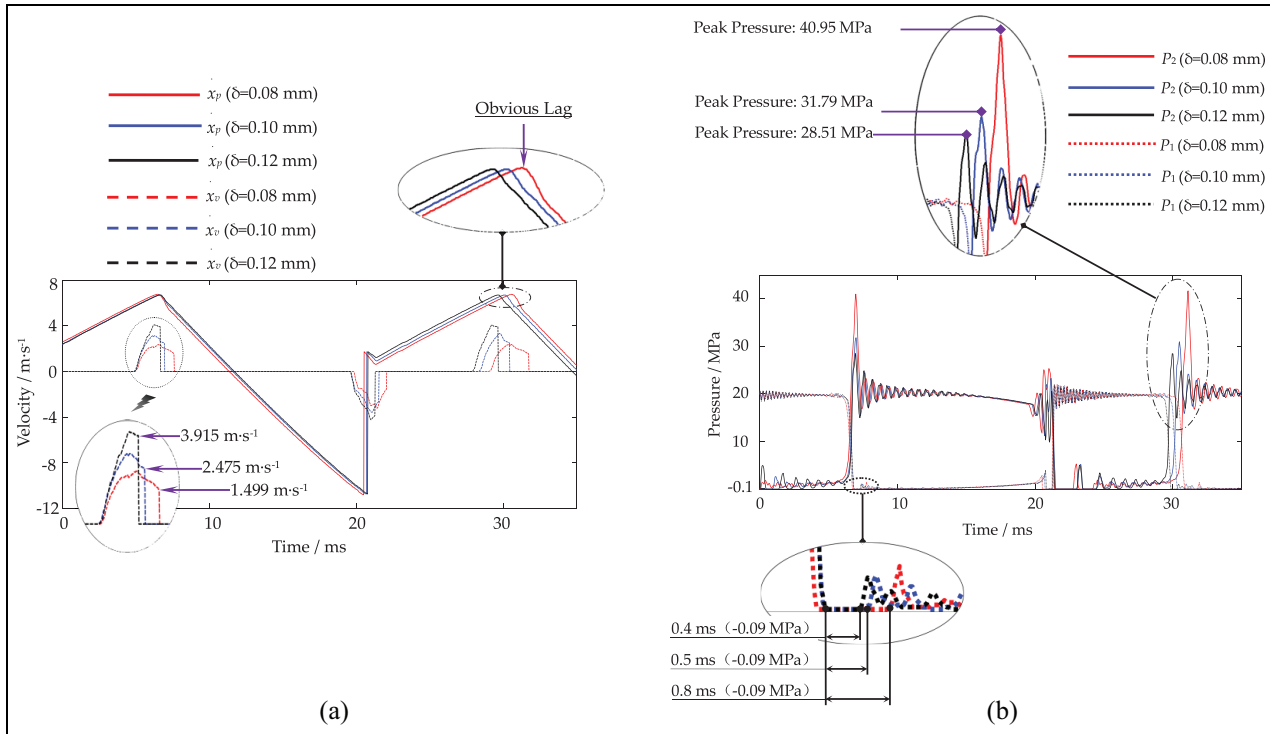


**Figure 10.** Simulation results of the percussion system with different  $\delta$  values: (a) velocity curves of the impact piston and spool valve; (b) pressure curves of impact piston's front-chamber and rear-chamber.

performance, but they do not reveal the rule by simulation. G Yang and colleagues<sup>32,33</sup> found the cavitation erosion phenomena of the impact piston and bush (Figure 9) in long-term use of rock drills, while they failed to find out the problem nature. The pressure and flow in the percussion system change greatly. The cavitation characteristics of system will be affected by the response of impact piston, which is related to the diameter of pipeline 1 and pipeline 2 (Figure 2). Therefore, the simulation will be carried out with different  $\delta$  and pipe diameters considering the capacity, resistance, and inertia.

#### Damping clearance of spool valve

The velocity curve of impact piston and spool valve, and the pressure curve of front-chamber and rear-chamber are obtained by simulation with different damping clearances of spool valve  $\delta$ , which is shown in Figure 10, and we can observe the following:

1. The damping clearance of spool valve ( $\delta$ ) has an important influence on the impact velocity and reversal time of spool valve. When  $\delta$  is 0.08, 0.10

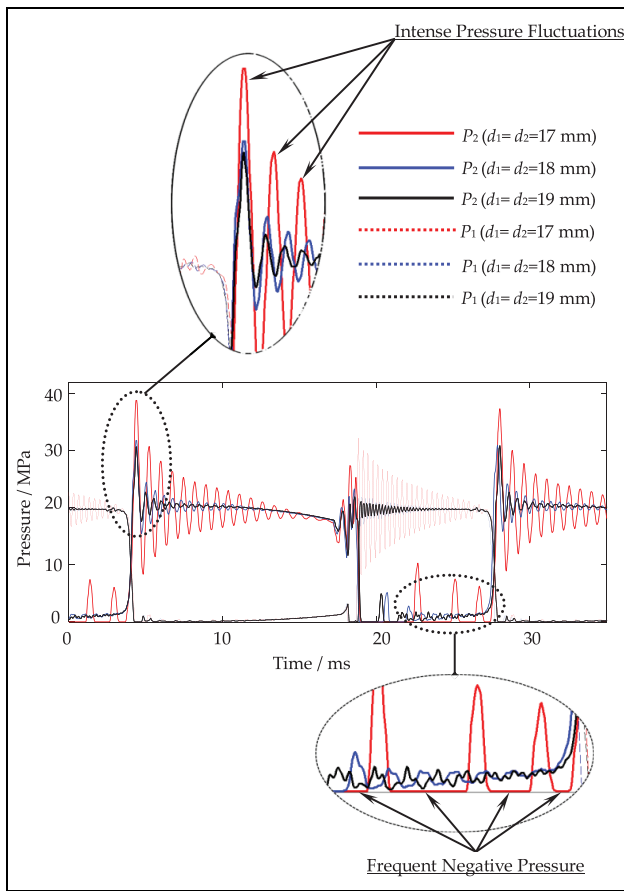


**Figure 11.** Simulation results of the percussion system with different diameters of connecting pipeline.

and  $0.12$  mm, the impact velocity of spool valve is  $1.499$ ,  $2.475$ , and  $3.915\text{ m s}^{-1}$ , and the reversal time of spool valve is  $2.8$ ,  $2.1$  and  $1.8$  ms.

2. The motion period of impact piston is affected because of variation of the spool valve's motion. When  $\delta$  is  $0.08$ ,  $0.10$ , and  $0.12$  mm, the motion period was  $24.1$ ,  $23.5$  and  $23$  ms, and the corresponding impact frequency of rock drill is  $41.49$ ,  $42.55$ , and  $43.48$  Hz.
3. During the braking phase of impact piston, the pressure fluctuation of rear-chamber ( $P_2$ ) will become severe when  $\delta$  is  $0.08$  mm, and the peak pressure can reach  $40$  MPa. Besides, the negative pressure ( $-0.09$  MPa) of front-chamber ( $P_1$ ) will last  $0.8$  ms, which is longer than that when  $\delta$  is  $0.10$  and  $0.12$  mm. This will aggravate the cavitation of percussion system.

It can be concluded that the larger  $\delta$  is better considering reversal time of spool valve, the impact frequency of rock drill, pressure fluctuation, and cavitation relief. But too large  $\delta$  will cause over quick impact velocity of the spool valve, which may lead to strong vibration and the damage of spool valve. Based on the above analysis, the damping clearance of spool valve  $\delta$  should be  $0.01$  mm by comprehensive consideration.

and the damage of spool valve. Based on the above analysis, the damping clearance of spool valve  $\delta$  should be  $0.01$  mm by comprehensive consideration.

### Connecting pipeline diameter

The simulation is carried out with different diameters of pipeline 1 and pipeline 2 (Figure 2) considering the capacity, resistance, and inertia. The results are shown in Figure 11, and we can observe the following:

1. The impact frequency of rock drill has little difference.
2. During the braking phase of impact piston, the pressure fluctuation in rear-chamber will become very severe when pipeline diameter is  $17$  mm. In contrast, the pressure fluctuation is stationary when pipeline diameter values are  $18$  and  $19$  mm.
3. When pipeline diameter is  $17$  mm, the negative pressure ( $-0.09$  MPa) in rear-chamber will appear continuously during the return acceleration phase of impact piston, which will aggravate the cavitation of percussion system.

It can be found that the pipeline diameter should be larger than  $18$  mm considering the pressure fluctuation and cavitation relief.

### Conclusion

1. The calculation formula of impact piston's rebound velocity was derived. The coupling model including impact piston, spool valve, impact accumulator, and connecting pipelines was established considering the structural feature and dynamic characteristics of the percussion system.
2. The pressure curves of impact piston's front-chamber and rear-chamber, valve's left-chamber and right-chamber were obtained by the field rock drilling test. The velocity curve of impact piston was acquired. The simulation and experimental results had consistency. The simulation model was verified.
3. The influence of damping clearance ( $\delta$ ) on the percussion performance was researched. The results show that the larger one is better considering reversal time of spool valve, the impact frequency of rock drill, pressure fluctuation, and cavitation relief. But too large one would cause over quick impact velocity of the spool valve, which may lead to strong vibration and the damage of spool valve. Based on the above analysis, the damping clearance of spool valve

- ( $\delta$ ) should be 0.01 mm by comprehensive consideration.
4. The cavitation erosion of the impact piston and bush is closely related to the damping clearance ( $\delta$ ) and pipeline diameters ( $\delta$ ). The negative pressure (-0.09 MPa) of front-chamber ( $P_1$ ) will last 0.8 ms when  $\delta$  is 0.08 mm. It is longer than that when  $\delta$  is 0.10 and 0.12 mm. This will aggravate the cavitation of percussion system. Besides, when the pipeline diameter is 17 mm, the negative pressure (-0.09 MPa) of rear-chamber will appear continuously during the return acceleration phase of impact piston, which will aggravate the cavitation of percussion system. The pipeline diameter should be larger than 18 mm considering the pressure fluctuation and cavitation relief.

### Declaration of conflicting interests

The author(s) declared no potential conflicts of interest with respect to the research, authorship, and/or publication of this article.

### Funding

The author(s) disclosed receipt of the following financial support for the research, authorship, and/or publication of this article: This research was funded by the National Key Research and Development Program of China (grant no. 2016YFC0802900), the Fundamental Research Funds for the Central Universities of China (grant no. FRF-TP-17-026A1), the General Financial Grant from the China Postdoctoral Science Foundation (grant no. 2017M620621), and the National Natural Science Foundation of China (grant no. 51774019).

### ORCID iDs

Wei Ma  <https://orcid.org/0000-0001-6176-9911>  
Xiaoguang Geng  <https://orcid.org/0000-0001-6393-6840>

### References

1. Oh J, Song C, Kim DJ, et al. Numerical investigation of performance of hydraulic percussion drifter. *Int J Precis Eng Manufact* 2016; 17: 879–885.
2. Shin DY and Kwon KB. A study on performance optimization of a hydraulic breaker. *Trans Korean Soc Mech Eng A* 2011; 35: 677–682.
3. Wang Y, Fang C, Jiang Q, et al. The automatic drilling system of 6R-2P mining drill jumbos. *Adv Mech Eng* 2015; 7: 504861.
4. Long R, Sun S and Lian Z. Research on the hard-rock breaking mechanism of hydraulic drilling impact tunneling. *Mathemat Prob Eng* 2015; 2015: 153648.
5. Peng J, Ge D, Zhang X, et al. Fluidic DTH hammer with backward-impact-damping design for hard rock drilling. *J Petrol Sci Eng* 2018; 171: 1077–1083.
6. Timonin VV, Alekseev SE, Karpov VN, et al. Influence of DTH hammer impact energy on drilling-with-casing system performance. *J Mining Sci* 2018; 54: 53–60.
7. Hwang UK and Lim JH. Optimization of down-the-hole hammer using experimental design method. *Trans Korean Soc Mech Eng A* 2016; 40: 603–611.
8. Song CH, Kwon KB, Shin DY, et al. Trend analysis of drilling technology for top-hammer drilling machine. *Tunnel Underground Space* 2013; 23: 271–279.
9. Zheng H, Zhao T and Li C. Research on high-speed photogrammetry for revolving-drilling tests. *J Vibrat Measure Diagn* 2015; 2: 339–344.
10. Li Y, Ma F and Geng X. Effect of annular clearance inside the double damping chamber on the dynamic characteristics of a rock drill damping system. *J Univ Sci Tech Beijing* 2014; 36: 1676–1682.
11. Seo J, Noh DK, Lee GH, et al. A percussion performance analysis for rock-drill drifter through simulation modeling and experimental validation. *Int J Precis Eng Manufact* 2016; 17: 163–170.
12. Seo J, Park JS, Kim H, et al. Experimental evaluation of percussion performance for rock-drill drifter. *J Biosyst Eng* 2015; 40: 1–9.
13. Noh DK, Seo J, Park JS, et al. Analysis of drifters critical performance factors using its hydraulic analysis model. *J Korea Soc Simulat* 2014; 23: 33–40.
14. Oh JY, Lee GH, Kang HS, et al. Modeling and performance analysis of rock drill drifters for rock stiffness. *Int J Precis Eng Manufact* 2012; 13: 2187–2193.
15. Oh JY, Lee GH and Song CS. A study on the analysis of hydraulic circuit of a rock drill drifter. *Proc KSFC Spring Conf* 2011; 2011: 70–75.
16. Hu Q, Yang C, Zheng H, et al. Dynamic simulation and test research of impact performance of hydraulic rock drill with no constant-pressurized chamber. *Automat Construct* 2014; 37: 211–216.
17. Yang S, Ou Y, Guo Y, et al. Analysis and optimization of the working parameters of the impact mechanism of hydraulic rock drill based on a numerical simulation. *Int J Precis Eng Manufact* 2017; 18: 971–977.
18. Guo Y, Liu D, Yang S, et al. Hydraulic-mechanical coupling modeling by bond graph for impact system of a high frequency rock drill drifter with sleeve distributor. *Automat Construct* 2016; 63: 88–99.
19. Guo Y, Liu D, Yang S, et al. Impact performance for high frequency hydraulic rock drill drifter with sleeve valve. *Int J Fluid Machine Syst* 2016; 9: 39–46.
20. Song C, Chung J, Cho J-S, et al. Optimal design parameters of a percussive drilling system for efficiency improvement. *Adv Mater Sci Eng* 2018; 2018: 1–13.
21. Li Y, Luo Y and Wu X. Impact system dynamic characteristics of hydraulic rock drill based on an overlapped reversing valve. *Shock Vibrat* 2018; 2018: 8963750.
22. Hu J and Hu Q. Oil pressure pulse features of a hydraulic impactor with an overlapped oil distributing valve. *J Vibrat Shock* 2014; 31: 73–78.
23. Zhao H, Fu S and Zhou M. Design and experiment on the opening at zero position of distribute valve of hydraulic rock drill. *Chin J Eng Design* 2016; 23: 288–294.

24. Ding W and Huang X. Modeling and simulation for a self-distributing flow hydraulic impactor. <i>J Vibrat Shock</i> 2010; 29: 103–106, 224.	$F_f$	friction force of the seal (N)
25. Zhou Z, Qin Z, Ma X, et al. Modeling and simulation of the impact of institutions of hydraulic rock drill based on AMESim. <i>Hydraul Pneumat Seals</i> 2010; 12: 11.	$h_5, h_6$	fit clearance (m) corresponding to $d_{v1}$ and $d_{v2}$
26. Yin Z and Hu Y. Dynamic simulation of the impact mechanism of hydraulic rock drill based on AMESim. <i>Adv Mater Res</i> 2012; 52: 1296–1300.	$h_i$	fit clearance (m) corresponding to $L_{pi}$ ( $i = 1, 2, 4$ )
27. Wen Z, Wang J, Yang S, et al. Modeling and simulation analysis on impactor hydraulic system of water-powered pile driver. <i>China Mech Eng</i> 2013; 24: 1809–1816.	$K$	load stiffness of rock ( $\text{N m}^{-1}$ )
28. Hashiba K, Fukui K, Liang YZ, et al. Force-penetration curves of a button bit generated during impact penetration into rock. <i>Int J Impact Eng</i> 2015; 85: 45–56.	$K_e$	oil elastic modulus (MPa)
29. Lundberg B and Huo J. Biconvex versus bilinear force-penetration relationship in percussive drilling of rock. <i>Int J Impact Eng</i> 2017; 100: 7–12.	$K_p$	viscous friction coefficient ( $\text{kg s}^{-1}$ )
30. Hashiba K, Fukui K, Liang YM, et al. Modeling of force-penetration curves for a button bit during impact penetration into rock. <i>Int J Rock Mech Mining Sci</i> 2017; 93: 210–214.	$K_v$	viscous friction coefficient ( $\text{kg s}^{-1}$ )
31. Li Y, Luo Y and Wu X. Fault diagnosis research on impact system of hydraulic rock drill based on internal mechanism testing method. <i>Shock Vibrat</i> 2018; 2018: 4928438.	$L_i, d_i$ ( $i = 1, 2$ )	length and diameter of pipelines (m)
32. Yang G, Xiang X and Guo S. Research on the cavitation damage of hydraulic rock drill. <i>Construct Machine Maintenance</i> 2017; 7: 43–45.	$L_h$	length of impact piston (m)
33. Yang G, Zhang F and Guo Z. Damage analysis of hydraulic rock drill's main parts. <i>Construct Machine Digest</i> 2015; 3: 91–94.	$m_p$	mass of impact piston (kg)
	$m_v$	mass of spool valve (kg)
	$P_i$	pressure (Pa) corresponding to $C_{vi}$ ( $i = 1, 2, 3, 4, 5, 6$ )
	$P_h$	pressure in oil chamber (Pa)
	$P_r$	incident stress wave (Pa)
	$Q_h$	flow rate into accumulator ( $\text{m}^3 \text{s}^{-1}$ )
	$Q_r$	reflected wave
	$R_i, C_i$ , and $I_i$ ( $i = 1, 2$ )	liquid resistance, liquid capacity, and hydraulic inductance of pipelines
	$u$	penetration depth (m)
	$u_A$	displacement of drill rod after unloading
	$V_H$	gas volume ( $\text{m}^3$ )
	$V_{H0}$	initial gas volume ( $\text{m}^3$ )
	$V_{i0}$	initial volume of $C_{vi}$ ( $i = 1, 2, 3, 4, 5, 6$ ) ( $\text{m}^3$ )
	$t_h$	duration of incident wave (s)
	$v_{pp}$	last impact velocity of impact piston ( $\text{m s}^{-1}$ )
	$Z_h, Z_q$	wave resistance ( $\text{Ns m}^{-1}$ ) of impact piston and shank adapter
	$\dot{x}_p, \ddot{x}_p$	velocity ( $\text{m s}^{-1}$ ) and acceleration ( $\text{m s}^{-2}$ ) of impact piston
	$\dot{x}_v, \ddot{x}_v$	velocity ( $\text{m s}^{-1}$ ) and acceleration ( $\text{m s}^{-2}$ ) of spool valve
	$\gamma$	unload coefficient
	$\delta$	damping clearance of spool valve
	$\varepsilon$	eccentricity
	$\mu$	dynamic viscosity of hydraulic oil ( $\text{kg}(\text{m s})^{-1}$ )
	$\zeta$	compressibility correlation coefficient of O-ring

## Appendix I

### Notation

$A_1, A_2$	effective area of the front-chamber and rear-chamber ( $\text{m}^2$ )
$A, E$ , and $\rho$	cross sectional area ( $\text{m}^2$ ), elastic modulus (Pa) and density ( $\text{kg m}^{-3}$ ) of impact piston
$A_{vi}$	effective area of spool valve ( $\text{m}^2$ )
$b$	seal width (mm)
$c$	wave velocity ( $\text{m s}^{-1}$ )
$C_3, C_4$	variables for state judgment (0 or 1)
$C_{v1}, C_{v2}$	front-chamber and rear-chamber of impact piston
$f$	is the friction coefficient between the seal and impact piston